ORIGINAL PAPER

A Critical View on the Quantification of Model Catalyst Activity

Johanna Reich[1] · Sebastian Kaiser[2] · Ueli Heiz[2] · Jan-Dierk Grunwaldt[3] · Manfred M. Kappes[4] · Friedrich Esch[2] · Barbara A. J. Lechner[1,5]

Abstract

The conversion of reactants, reaction rate referred to catalyst mass, and turnover frequency (TOF) are values typically employed to compare the activity of different catalysts. However, experimental parameters have to be chosen carefully when systems of different complexity are compared. In order to characterize UHV-based model systems, we use a highly sensitive sniffer setup which allows us to investigate the catalytic activity by combining three different measurement modes: temperature-programmed desorption, continuous flow, and pulsed-reactivity experiments. In this article, we explore the caveats of quantifying catalytic activity in UHV on the well-studied and highly defined reference system of CO oxidation on Pt(111), which we later compare to the same reaction on Pt_{19} clusters deposited on $Fe_3O_4(001)$. We demonstrate that we can apply fast heating ramps for TOF quantification, thus inducing as little sintering as possible in the metastable clusters. By changing the reactant ratio, we find transient reactivity effects that influence the TOF, which should be kept in mind when comparing catalysts. In addition, the TOF also depends on the surface coverage that itself is a function of temperature and pressure. At a constant reactant ratio, in the absence of transient effects, however, the TOF scales linearly with total pressure over the entire measured temperature range from 200 to 700 K since the reaction rate is dependent on both reactant partial pressures with temperature-dependent reaction order. When comparing the maximum TOF at this particular reactant ratio, we find a 1.6 times higher maximum TOF for $Pt_{19}/Fe_3O_4(001)$ than for Pt(111). In addition, pulsed-reactivity measurements help identify purely reaction-limited regimes and allow for a more detailed investigation of limiting reactants over the whole temperature range.

Keywords Heterogeneous catalysis · Catalytic activity · Cluster catalysts · Turnover frequency · Magnetite · Temporal analysis of products

Johanna Reich and Sebastian Kaiser have equally contributed to this work.

✉ Friedrich Esch
   friedrich.esch@tum.de

✉ Barbara A. J. Lechner
   bajlechner@tum.de

1 Department of Chemistry, Functional Nanomaterials Group and Catalysis Research Center, School of Natural Sciences, Technical University of Munich, 85748 Garching, Germany

2 Department of Chemistry, Chair of Physical Chemistry and Catalysis Research Center, School of Natural Sciences, Technical University of Munich, 85748 Garching, Germany

3 Institute for Chemical Technology and Polymer Chemistry, Karlsruhe Institute of Technology, 76131 Karlsruhe, Germany

4 Institute of Physical Chemistry, Karlsruhe Institute of Technology, 76131 Karlsruhe, Germany

5 Institute for Advanced Study, Technical University of Munich, 85748 Garching, Germany

1 Introduction

A selective application-tailored design of heterogeneous catalysts would be an optimal way of minimizing cost and maximizing material efficiency in any kind of application, ranging from chemical industry to emission control. Fundamental research on the nanoscale aims at obtaining a relationship between structure and reactivity of catalytic systems on an atomic level by investigating model systems with reduced complexity under highly defined conditions in ultrahigh vacuum (UHV) [1, 2], ambient [3, 4] and even at elevated pressures [5]. Determining catalytic activity in UHV-based model system studies can provide valuable fundamental information, since the systems are as highly defined as possible—ideally, the number of active sites is known exactly or comparatively easy to estimate by a broad variety of characterization techniques. Those results can then help more application-oriented catalysis to understand

underlying processes and thus also have a technical impact. In order to legitimately compare the results from UHV conditions with catalytic tests under real operating conditions [6, 7], there are two commonly applied quantification parameters. The turnover frequency (TOF) is defined as the number of product molecules per time interval and active site [8],

$$TOF = \frac{\dot{N}_{prod}}{N_{active\ sites}}[s^{-1}]. \qquad (1)$$

Alternatively, catalytic activity can be qualitatively compared via the light-off temperatures measured at certain conversion values (e.g. T_{50} for 50% conversion) [9, 10]. However, the latter approach is applicable only if series of samples are evaluated and the testing conditions are the same. Furthermore, reaction rates referring to the mass of the active metal, catalyst mass or catalyst volume are used if the number of active sites is unknown.

In a larger collaborative research initiative (CRC1441, details see Ref. [11]), we aim at comparing catalytic activity over large complexity and pressure ranges, from size-selected sub-nanometer clusters on single crystalline supports to applied powder and monolithic catalyst systems. While pressure and temperature dependent, the TOF is preferred when it comes to comparing reaction rates across systems of different complexity, since it already contains the number of active sites [12]. However, the reaction rate and thus the TOF depend on the reaction conditions [7]. In addition, the comparison across such a large parameter range is inherently challenging [12–14]. We need to pay particular attention to several caveats. First of all, the number of active sites has to be quantified precisely, which is easy for model systems, but may become more complicated for applied and powdered catalysts. Ideally, the quantification procedure should not involve sample pre-treatment steps that change the structure of the active species prior to the measurement itself. A second point regards mass transport limitations (MTL) [15], which alter the apparent catalytic activity at the active site and thus the estimated TOF by hampering the reactant and product transport to and from the active site. External MTL concerns the transport of reactants from the gas phase on the surface [16], and is a major factor especially in the low partial pressure regime and has to be taken into account when comparing catalytic activity across different pressures and when the reaction rate is high compared to the diffusion. On the other hand, internal MTL, i.e. the diffusion of reactants and products into and out of the catalyst interior (pore diffusion) [17], depend strongly on the complexity of the system: We can rule it out on extended single crystal surfaces, where rate limitation is dominated by surface reconstructions [18], island formation [19], or blocking of active sites [5, 20]. For clusters or nanoparticles deposited on single crystal oxides, the activity is still not

affected by internal MTL, but now we additionally introduce rate-limiting effects like spillover [21], sintering [22], restructuring of the particles [23] or strong metal-support interaction (SMSI) [3] while performing catalytic measurements. Internal MTL comes into play if we investigate powder catalysts, but here its extent strongly depends on the thickness of the catalyst layer, the reaction rate and grain size [7, 15]. Minimizing MTL effects requires catalytic testing in thin layers and at low conversions, where temperature gradients are also minimized [6, 7, 15].

A third caveat is the entangled pressure and temperature dependence of the reaction light-off, e.g. a reactant ratio dependence that varies with total pressure and temperature [4, 24–26]. This explains the seemingly strong variations of TOF values in the literature and requires a reasonable choice of temperature and pressure to compare similar reaction regimes. At high temperatures, the reaction rates are fast, but at the same time the surface coverages may become small. Hence, it is often wise to determine the TOF over a certain temperature range in order to unravel trends and structure–reactivity relationships, as we aim to conduct here. It is difficult to adequately consider all these three aspects at the same time; in particular, the pure reaction-controlled regime may be achieved only in a narrow temperature window and comparability cannot always be reached.

In this work, we address catalytic activity of model systems of different complexity in a UHV-based reactor setup, starting from the prototypical CO oxidation on Pt(111) as reference [14, 19] and later performing the same reaction on monodisperse Pt_{19} clusters deposited on $Fe_3O_4(001)$. We use a simple "sniffer" setup, developed by Bonanni et al. [27], which allows for highly sensitive product analysis and pulsed reactant dosing, thus acting as a so-called "temporal analysis of products" (TAP) reactor under UHV and low pressure conditions. Thanks to the high sensitivity, the sniffer gives access to TOF determination even on ultimately flat catalytic surfaces with a low number of active sites and with maximum control on catalyst composition and structure. With this setup, three distinct measurement modes can be achieved and switched between rapidly: (i) Highly sensitive temperature-programmed desorption (TPD) measurements allow us to determine available adsorption sites, desorption energies and desorption mechanisms. In our work, we use this measurement mode for sensitivity calibration. (ii) Continuous flow measurements under isothermal and temperature-programmed reaction (TPR) conditions are used to determine TOF numbers under steady-state conditions. Here, reactant pressure modulations allow to determine mass transport limitations. (iii) Pulsed-reactivity measurements, where the reactants are pulsed continuously at variable temperatures, provide a snapshot of the system that indicates limiting reactants and their influence on selectivity, transport limitations, adsorption–desorption equilibria and spillover

phenomena [21, 27, 28]. This toolbox of the three combined measurement modes makes it possible to clearly identify the parameter range of the catalytic regime of interest and hence confines the limits of validity and comparability of specific TOF numbers, as will be explored within this article.

2 Experimental Methods

2.1 The Sniffer Setup

The sniffer setup was adapted from a design by Bonanni et al. [27]. In its core, it consists of a trident-shaped quartz tube assembly that guides reactant gases from two pulsed solenoid valves to the sample surface and the product and reactant mixture through a central tube to the differentially pumped ionization region of a quadrupole mass spectrometer (QMS). The whole quartz assembly is heated to $\geq 150\ °C$ in order to prevent gas molecules from sticking to the walls and terminates with a quartz cone adjusted to the sample size (opening 3 mm, wall thickness 1 mm, sample diameter 4.4 mm) which is positioned reproducibly at $250 \pm 50\ \mu m$ above the sample, thus maximizing the sensitivity and minimizing background signals. Elevated pressures are feasible with the given tube diameters and ionization window geometry, but we limit the pulse pressures to the 10^{-5} mbar range to stay within the specifications of the QMA 200 Prisma Plus (Pfeiffer Vacuum GmbH). In our adaptation of the design, the lines are filled with a pressure of 1 mbar of the dosed gases to ensure low contamination from the gas supply system and can thus act as a compact reservoir for costly isotopically labelled gases. Furthermore, we enlarged the dimensions of the dosing tubes compared to ref. [27] and inserted bellow-sealed valves (Swagelok, H Series) between the solenoid valves for gas pulsing (Parker Series 99) and the sniffer for easier servicing, which does not affect the pulse shapes. Finally, we went back from slits to the original Pfeiffer geometry of the apertures through which the electrons are transferred from the filament to the ionization region to strongly enhance the sensitivity while reducing background signals by electron impact. Further details are given in Fig. S1 in the electronic supporting information.

2.1.1 Pulsed-Reactivity Measurements

With the sniffer setup, pulsed-reactivity measurements can be performed either with (i) alternating reactant pulses with a varying pulse frequency, delay time and gas pressure ratio, (ii) simultaneous reactant pulses with varying frequency and gas ratio or (iii) constantly dosing one reactant in the background while pulsing the other reactant. The pulse height (proportional to gas throughput—see below) is controlled via the voltage applied to the solenoid valves, while we kept

the opening time of the valves constant at 5 ms (SI, Fig. S2). As observed by Harbich and coworkers, mounting the solenoid valves against the indicated flow direction allows us to work with these very short response times [private communications].

It is important to note that not all of the gas contained in one pulse reaches the surface. To quantify this effect, we pulsed CO onto a CO-precovered Pt(111) single crystal while gradually retracting the sample from the sniffer cone until the pulses are no longer reflected by the surface (SI, Fig. S3) and determined the proportion of reactants reaching the catalyst to be about 35%.

In the QMS, the pulses always appear with a sharp increase in signal, followed by a decaying "tail", which is not only influenced by the gas-dependent pumping efficiency, but also contains information on adsorption/desorption equilibria. Typical decay times of weakly interacting gases are around 600 ms, such as O_2 measured at 5% of the pulse maximum for a maximum pulse pressure of $1.5 \bullet 10^{-7}$ mbar on a CO poisoned Pt(111) surface at 200 K.

Naturally, the total amount of gas dosed onto the surface per pulse strongly depends on the pulse height. For example, a typical CO pulse with a maximum of $1.8 \bullet 10^{-6}$ mbar corresponds to 0.07 L, as quantified by comparison to CO TPD measurements of the CO-saturated Pt(111) surface with a known coverage (SI, Fig. S4). To obtain a higher signal-to-noise ratio, we apply isotopically labelled gases that appear at m/z values with lower background signal. All pulsed-reactivity measurements in this article have been measured with $C^{18}O$ (m/z = 30) and $^{16}O_2$ (m/z = 32), which leads to CO_2 being detected as $C^{16}O^{18}O$ (m/z = 46). Integration of the pulse signals of reactants and products was performed using a home-written MATLAB routine, which is described elsewhere [21].

Prior to the pulsed-reactivity experiments, the QMS signal was calibrated against pressure via calibration curves by dosing varying gas pressures in the chamber background while closing off the differential pumping in order to ensure homogeneous gas distribution in the sniffer and the rest of the chamber. The chamber pressure was measured using a Bayard-Alpert hot cathode gauge (AML). Note that it is important to correct for gas dependent gauge sensitivity factors [29] (1.05 for CO, 1.01 for O_2 and 1.42 for CO_2 [30, 31]).

2.1.2 Continuous Flow Measurements

Continuous flow measurements for a quantitative analysis of catalytic activity were performed by backfilling the UHV chamber (base pressure $< 2 \bullet 10^{-10}$ mbar) with the reactant gases (in this case CO and O_2) at pressures between 10^{-9} and 10^{-6} mbar. Here, the gases leak through the small gap between sniffer and sample, leading to a pressure drop from

the UHV chamber to the catalyst surface under the sniffer and further to the differentially pumped QMS. The pressures indicated in the following are partial pressures at the catalyst surface converted from measured QMS signals by (i) referencing the QMS signals to the UHV chamber pressures and (ii) taking into account that only $57 \pm 12\%$ of the reactant pressures in the UHV chamber reach the sample surface (for details see SI, Section S5). Note that due to the size of the chamber non-isotopically labelled gases were used for continuous flow measurements. Furthermore, using isotopically labeled reactants at increased pressures also increases the background signal of isotopically labeled CO_2 product molecules and thus reduces the benefit of performing isotopically labeled experiments.

The calculation of the TOF as in Eq. (1) requires a precise determination of the molar flow of a selected reactant (here CO) to calculate the molar flow of the product and of the number of active sites.

The molar flow of the reactant CO is calculated from the QMS signal by evaluating a CO TPD from Pt(111), which reaches a maximum coverage of $\theta = 0.5$ at 200 K [32]. Calibration TPD measurements were performed by saturating the surface with $C^{18}O$ (typically 100 pulses of 0.07 L each) and applying a heating ramp of 1 K/s up to 573 K. Since the sniffer cone is placed very close to the surface, we assume that only molecules desorbing from the area below the cone are measured in the QMS. With a cone diameter of 3.0 mm and a Pt(111) atom density of $\rho = 1.5 \bullet 10^{15} cm^{-2}$ [32], we obtain a total number of $N_{COsat} = \theta_{CO} \bullet N_{surface} = 5.03 \bullet 10^{13}$ corresponding to the integral of the QMS signal for a saturated CO TPD. From Eq. (2) below, we obtain the molar flow of CO, given in molecules per second. The term $I_{28} - I_{28bg}$ corresponds to the background-corrected CO-QMS signal and Q_{TPD} is the integral of the saturated, background-corrected CO TPD.

$$
\begin{aligned}
\dot{N}_{CO}\left[s^{-1}\right] &= N_{COsat} \bullet \frac{\left(I_{28} - I_{28bg}\right)[A]}{Q_{TPD}[As]} \\
&= a_{QMS_{CO}}[A^{-1}s^{-1}] \bullet (I_{28} - I_{28bg})[A]
\end{aligned}
\tag{2}
$$

The molar flow of the product CO_2 is obtained analogously, including the QMS sensitivity factors s_{QMS} for CO and CO_2,

$$
\dot{N}_{CO_2}\left[s^{-1}\right] = \frac{s_{QMS_{CO_2}}}{s_{QMS_{CO}}} \bullet a_{QMS_{CO}}[A^{-1}s^{-1}] \bullet \left(I_{44} - I_{44bg}\right)[A].
\tag{3}
$$

On our well-defined model systems, the number of active sites is determined purely by geometric considerations, i.e. assuming that all atoms are active sites: For single crystals, the number of active sites thus equals the number of surface atoms below the sniffer cone, calculated as described

above. For clusters with fewer than 20 atoms, the dispersion $D = \frac{N_{surface}}{N}$ is close to 1, which lets us assume that nearly every atom of the clusters represents a surface atom and thus an active site[1]; the cluster coverage is precisely known from the deposition current. For larger nanoparticles with a less well-defined number of atoms, one has to estimate the number of active sites from the particle size and shape, which can be obtained for example by electron microscopy [33].

With the above values, we calculate the TOF according to Eq. (1). Furthermore, we can additionally estimate the conversion by dividing the TOF value, obtained for a given temperature, by the impingement rate Z of the limiting reactant.

Continuous flow experiments were performed either in TPR or isothermal measurement mode. For TPR measurements, we applied heating and cooling ramps of 1 K/s with a short isothermal region of constant temperature at the highest and the lowest temperatures between the ramps. Isothermal measurements, in contrast, were performed by stepwise heating and a collection time of two minutes at each step as soon as temperature stabilization was reached.

2.2 Sample Preparation

A Pt(111) crystal (from Surface Preparation Laboratory) was prepared by cycles of Ar^+ sputtering ($4 \bullet 10^{-5}$ mbar Ar, 1 kV, 5 min) followed by annealing in UHV (1223 K, 5 min) in order to obtain a flat surface, another annealing step in an O_2 atmosphere ($5 \bullet 10^{-7}$ mbar O_2, 723 K, 10 min) to remove carbon and a final UHV annealing step (1003 K, 3 min) to desorb the remaining oxygen. Immediately before each measurement, the sample was flash annealed to 523 K to desorb CO covering the surface. The $Fe_3O_4(001)$ support (from SurfaceNet GmbH) was prepared via multiple cycles of Ar^+ sputtering ($4 \bullet 10^{-5}$ mbar Ar, 1 kV, 20 min) and annealing in O_2 ($5 \bullet 10^{-7}$ mbar O_2, 983 K, 20 min). The sample was flash annealed to 773 K before cluster deposition. The samples were heated using a boron nitride heater in direct contact and the temperature was measured via a type K thermocouple attached to the crystal, calibrated to a measurement accuracy of ± 5 K. Reactivity and TPD measurements were started at a temperature of 200 K, upon cooling the manipulator head with liquid N_2, and the cooling rate kept constant throughout the measurement.

Size-selected clusters were generated with a laser ablation cluster source [34] connected to the UHV chamber. Pt is ablated from a rotating target using the second harmonic of a pulsed Nd:YAG laser. The thus created plasma is rapidly cooled via adiabatic expansion of pulsed He seed gas

---

[1] Taking into account geometrical considerations, a Pt_{20} cluster of 2–4 layers height contains at maximum 2–3 non-surface atoms, leading to a minimal dispersion of 0.85.

(Westfalen AG, grade 6.0). This leads to the formation of a broad distribution of cluster sizes. Via electrostatic lenses, the resulting cluster beam is guided into a 90° bender which selects the cationic clusters and subsequent mass selection is obtained by a quadrupole mass filter. Applying a retarding voltage to the sample ensures soft-landing of the clusters ($E_{kin} < 1$ eV/atom) on the $Fe_3O_4(001)$ surface. The neutralization current is measured to quantify the cluster coverage.

2.3 STM Measurements

STM measurements were performed by transferring the samples into a UHV chamber directly connected to the sniffer setup (base pressure of $< 3 \bullet 10^{-11}$ mbar), using a Scienta Omicron VT-AFM instrument in constant current mode with homemade etched tungsten tips. Acquired images were processed using Gwyddion [35], applying mean plane subtraction, row aligning by median of differences and three-point plane levelling.

3 Results and Discussion

3.1 Isothermal CO Oxidation vs. Temperature-Programmed Reaction (TPR)

The dispersion D of clusters and nanoparticles has a significant influence on catalytic activity [36, 37]. When characterizing catalytic activity of small metastable particles for screening purposes, one has to make a tradeoff between a sufficiently short measurement time to keep particle sizes stable [22, 38–40] and time-consuming isothermal measurements, which are the accepted best practice in applied catalyst testing [6, 7]. Therefore, our first test is to check whether isothermal measurements are consistent with TPR ramps on the order of 1 K/s, typical for UHV experiments.

To this purpose, we study the CO oxidation on an extended Pt(111) surface as reference system and take care to discuss only the TPR signals from a second run, where initial adsorbate heterogeneities (SI, Fig. S5) have been overcome at the transition to higher temperatures. In Fig. 1 (a), we compare the TOF in the TPR measurement (blue line) to that of the isothermal measurement (black dots), where the sample was heated stepwise (temperature kept constant for 2 min after stabilization). Both gases, first CO, then O_2, were background dosed onto the sample at 200 K. Here, we use a gas mixture of 10% CO and 90% O_2 at a total gas pressure of $p_{sample} = 6.2 \bullet 10^{-7}$ mbar. As can be seen clearly, both coincide perfectly under these reaction conditions, which shows that we indeed reach quasi-isothermal conditions during fast heating ramps. Interestingly, the two curves show a light-off temperature around 380 K, which is approximately 100 K lower than values obtained at near-ambient pressures
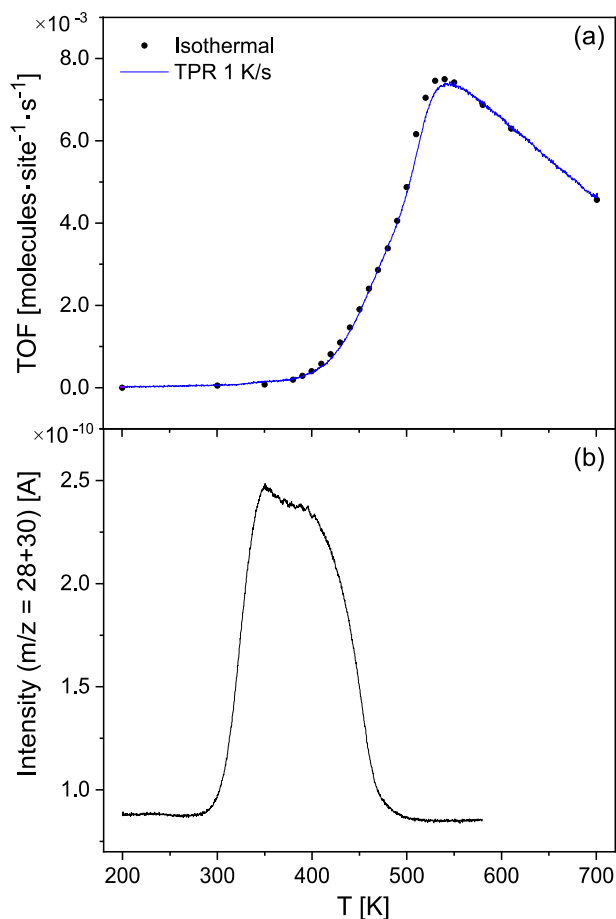
Fig. 1 a CO_2 production from CO oxidation on Pt(111) in continuous flow experiments ($p_{sample} = 6.2 \bullet 10^{-7}$ mbar with 10% CO and 90% O_2). Black dots: Isothermal measurements (2 min dwell time each). Blue curve: TPR run with a 1 K/s ramp. The isothermal curve is scaled to the TPR curve at 700 K (scaling factor: 0.88) to account for slight variations in the sniffer-sample distance. **b** CO TPD from a Pt(111) surface with 1 K/s. The surface was first saturated to a coverage of 0.5 ML with $C^{18}O$ by pulsing 100 pulses of approximately 0.07 L each at 200 K

between $1 \bullet 10^{-3}$ and 1 mbar at varying partial pressures [4, 41]. In a recent study by Blomberg et al., who studied CO oxidation on Pd(100), an exponential dependence of the light-off temperature on the CO partial pressure (10^{-6} mbar up to 1 bar, 1:1 ratio) was found in a temperature range between 200 and 405 K [42]. A higher CO background pressure shifts the equilibrium of CO desorption to higher temperatures and thus limits the availability of free O_2 adsorption sites, while O_2 needs two separate neighboring adsorption sites for dissociation [5, 43, 44]. Indeed, the comparison with the CO TPD in Fig. 1 (b) makes evident that the reaction starts above the desorption onset but still below complete desorption which enables an adsorption–desorption equilibrium. Note that the difference in the temperature windows is determined by the difference in the kinetic

conditions under which the three measurement types occur. The steepest slope is reached as soon as CO desorption is complete around 500 K, indicating that the reaction rate is limited by CO poisoning and that we are thus in a regime controlled by microkinetics up to this point.

The maximum rate is observed at 540 K with a TOF value of $7.5 \cdot 10^{-3}$ molecules$\cdot$site$^{-1} \cdot$s^{-1}. For the given pressure and a gas phase temperature of 298 K, the impingement rate of CO on the area below the sniffer cone equals $Z_{CO} = 0.016$ s$^{-1} \cdot$site^{-1}, implying a conversion of approximately 53%. At temperatures between 540 and 700 K, the TOF decreases again. Within this temperature region, the residence time of CO decreases exponentially with temperature [45] while O is typically present on the surface in the form of atoms and starts desorbing from 600 K [46]. The CO_2 production thus decreases due to an increasingly empty surface. We can additionally exclude O poisoning in this temperature region since the TOF recovers in a subsequent cooling ramp (SI, Fig. S6).

3.2 Exploring the Limits of TOF Quantification

In the previous section, we have shown that we can reach a quasi-isothermal steady state upon applying TPR ramps for TOF quantification. However, care has to be taken when applying this method as it reaches its limits as soon as transient reactivity peaks are involved, where the system is not in a steady state (Fig. 2 (a)). Here, we show a series of TPR measurements with varying gas compositions. The CO pressure was kept constant, while the O_2 pressure was gradually increased. The TPR measurements consist of a 1 K/s heating (intense colors) and a corresponding cooling ramp (light colors). Comparing both curves, for the lowest O_2 partial pressure (grey curves) we do not observe a significant change in the curve shape and only a small temperature hysteresis. For this gas phase composition, the TPR curve is exactly comparable to the isothermal measurement (Fig. 1 (a)). Doubling the amount of O_2 leads to an increase in overall CO_2 formation. However, when doubling the O_2 amount again, the CO_2 formation is roughly comparable to the intermediate case, in particular in the temperature range above 500 K. Here, the TOF saturates, indicating that the reaction is now limited by the supply of CO from the gas phase and no longer by the availability of O_2, as was the case for the grey curve.

At the same time, we observe a drastic change in the curve shape at lower temperatures. (i) Around 280 K, a low temperature CO_2 formation peak arises during the heating ramp, which resembles the actual onset temperature of the reaction when CO and O are co-adsorbed on the Pt surface [47]. We do not observe this feature in a more O_2 deficient environment (grey curve), where CO poisoning dominates, rendering the dissociative adsorption of O_2 impossible, as
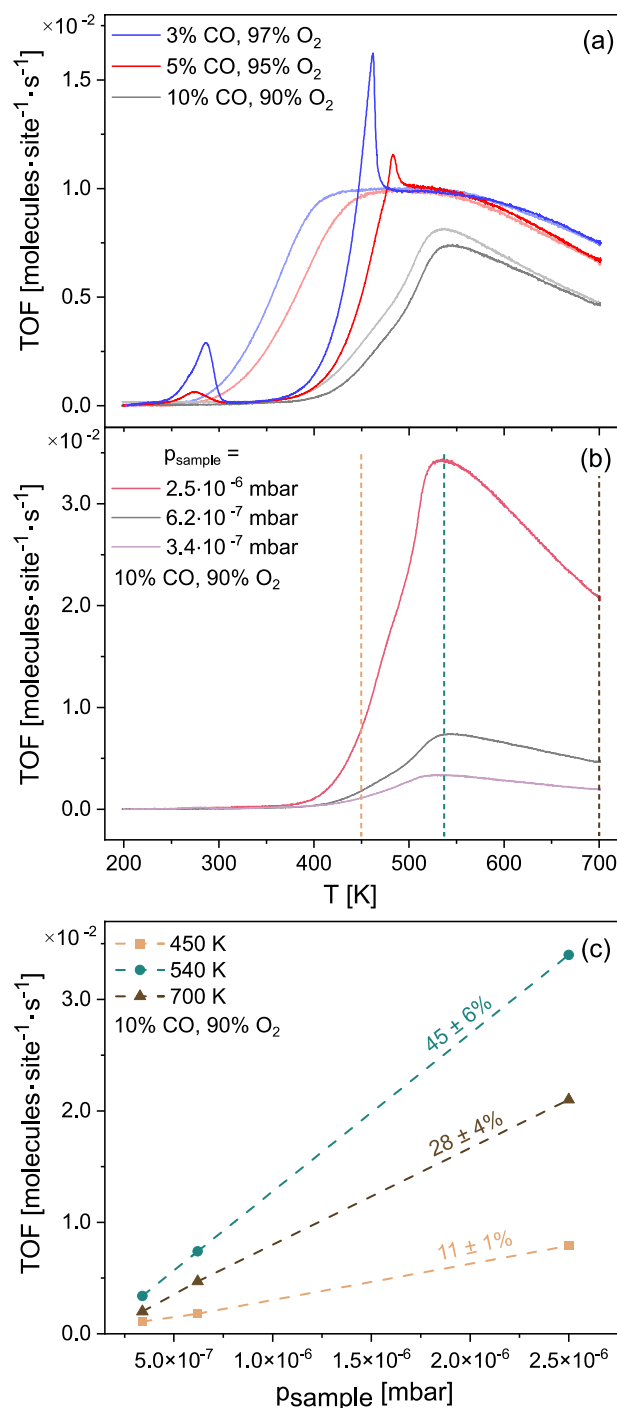
Fig. 2 CO_2 production from CO oxidation on Pt(111) in continuous flow experiments with temperature ramps of 1 K/s. **a** Variation of the O_2 pressure while the CO pressure is kept constant at $p_{CO,sample} = 8.5 \cdot 10^{-8}$ mbar. Dark colors: heating ramps. Bright colors: Corresponding cooling ramps. **b** Variation of the total pressure at a constant CO to O_2 ratio of 10 to 90%. **c** TOF at different temperatures and pressures, taken at different temperatures, see dashed lines in (**b**)

already shown in Fig. 1. Indeed, comparing the red and blue curves, we see that the intensity of the low-temperature peak scales with the amount of available O_2. As reported by Kinne et al. [48] and Wintterlin et al. [47], O atoms form dense islands with a (2×2) structure and the reaction with co-adsorbed CO takes place at their perimeter. (ii) For the two measurements with increased O_2 pressures (red and blue curves) the TOF maximum appears as a sharp peak, which is not observed in the corresponding cooling curves. In line with Gao et al. [41], we therefore assign this feature to a transient reactivity that is not observable during steady state measurements. (iii) Upon cooling, a significant hysteresis is observed for the red and blue curves. In contrast to the heating curve, the reactivity is not suppressed by CO poisoning in the cooling measurement, while oxygen is available in excess and readily participating in the reaction. Thus, CO_2 formation is observed down to the onset of the low temperature reaction feature.

To investigate whether these effects actually depend on gas ratio and not only total pressure, we performed another TPR measurement series at a constant reactant ratio while varying the overall gas pressure (Fig. 2 (b)). We stick to a gas composition of 10% CO and 90% O_2, where isothermal and TPR measurements were comparable (Fig. 1 (a)) and no clear transient effects were observed (Fig. 2 (a)). When increasing the overall pressure from $3.4 \cdot 10^{-7}$ to $6.2 \cdot 10^{-7}$ and $2.5 \cdot 10^{-6}$ mbar, the overall curve shape remains similar but the TOF scales with pressure. In order to take a closer look at the scaling behavior of the curve, we compare three temperatures: 450 K (within the reaction light-off), 540 K (at the TOF maximum) and 700 K (at the high-temperature limit). Fig. 2 (c) shows the TOF at different pressures, extracted along the vertical dashed lines (representing the above-mentioned temperatures). The TOF increases linearly with reactant pressure, which is connected to the equilibrium constant of reactant adsorption. An increased reactant partial pressure leads to an increased reactant coverage and thus, assuming the Langmuir–Hinshelwood mechanism, a higher total CO_2 production. It thus appears as though the additional CO molecules react off immediately with a conversion probability that depends solely on the CO residence time.[2] Since CO is continuously dosed, the TOF maximum appears at a temperature above the TPD desorption.

In order to explore this hypothesis, we now check the TOF and conversion for a supported cluster catalyst, i.e. Pt_{19} deposited on $Fe_3O_4(001)$ with a cluster coverage of 0.1 clusters/nm^2, which is the equivalent of an atom density of 13% of a Pt(111) monolayer. By employing cluster catalysts, we ensure that neither CO nor O_2 can form island superstructures. Furthermore, here CO has a higher activation energy for desorption, which is why the CO desorption is complete at approximately 70 K higher temperatures with respect

to a Pt(111) catalyst [21]. On the one hand, this leads to a stronger self-inhibition by poisoning at low temperatures on the cluster sample than on the extended Pt(111) surface, but on the other hand it may result in higher residence times for CO at elevated temperatures and thus a higher reaction probability at the same temperature, resulting in a higher maximum TOF.

In Fig. 3a we see comparable shapes of the light-off curve for $Pt_{19}/Fe_3O_4(001)$ and Pt(111), but with a shifted onset. The dark and bright blue TPR curves represent the first and second run, respectively, while the grey curve is the second TPR run on Pt(111); all curves are measured with the same settings as in Fig. 1. As expected for a sample with longer CO residence times, the maximum TOF for the first TPR run on Pt_{19} is indeed higher than that for Pt(111), by a factor of 1.6 for this specific cluster coverage. The TOF might even be increased by lowering the cluster coverage and thus maximizing the reverse spillover from the support to each active cluster (larger capture zone). In addition, the support may also play an important role in the catalytic activity, especially when it comes to reducible oxides. Gänzler et al. showed that CO oxidation on Pt/CeO_2 (reducible support) is enhanced towards Pt/Al_2O_3 (non-reducible support) due to the participation of interface O from the support in the reaction [49, 50]. Indeed, in earlier work, some of the authors showed that CO oxidation on $Pt_{19}/Fe_3O_4(001)$ equally occurs not only as a classical Langmuir–Hinshelwood mechanism but also as a Mars-van-Krevelen mechanism via lattice oxygen reverse spillover [21]. This could equally explain this enhanced TOF, since a higher O availability also leads to an increased maximum TOF, as we have shown above.

In contrast to the TPR measurements on Pt(111), the activity beyond the temperature of the TOF maximum decreases much more quickly and the second run shows a significantly lower activity than the first one. By comparing STM images of Pt_{19} as deposited (Fig. 3b) and after CO oxidation (Fig. 3c), we rule out severe sintering as a reason for the decreasing activity, since the apparent height of most clusters remains comparable to that of the as-deposited ones. (Note that in comparison to their real size the clusters appear laterally more extended in STM images due to a convolution with the tip shape and electronic effects.) The magnetite islands formed in Fig. 3c result from an O excess and are formed with Fe from the bulk [51]. In previous TPD and XPS experiments, we have shown that Pt clusters on $Fe_3O_4(001)$ undergo a strong metal-support interaction (SMSI)-induced encapsulation by a thin FeO-like layer [22], which deactivates them for CO adsorption and thus results in

---

[2] At such a high temperature, the reaction order is $+1$, in contrast to -1 at low temperatures, where the CO coverage is too high [7].
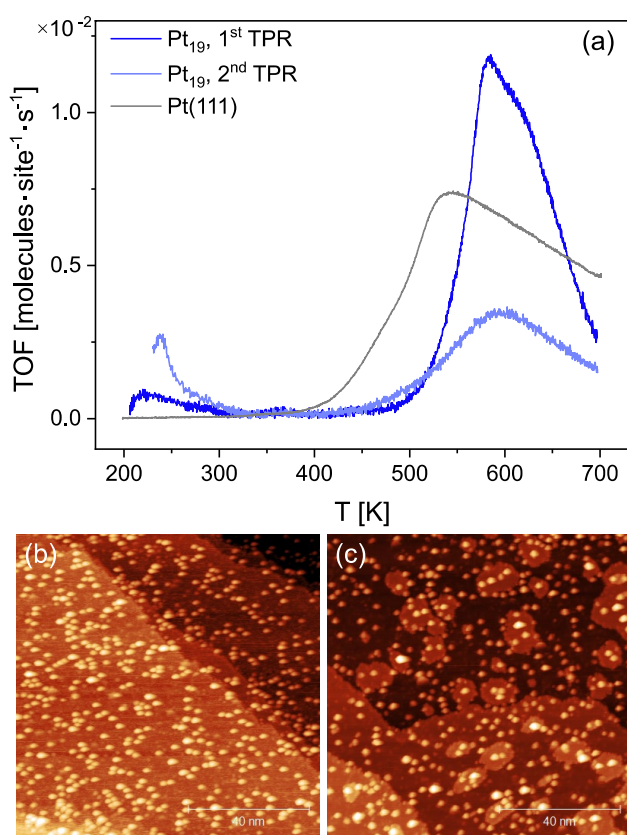
Fig. 3 **a** Continuous flow TPR measurement of CO_2 production during CO oxidation on Pt_{19} clusters on $Fe_3O_4(001)$ with a nominal cluster coverage of 0.1 clusters/nm² during a linear heating ramp of 1 K/s. Pressures are the same as in Fig. 1 ($p_{sample}=6.2 \cdot 10^{-7}$ mbar, 10% CO, 90% O_2), with CO dosed before O_2 at 200 K. **b** STM image of 0.05 clusters/nm² Pt_{19} as deposited on $Fe_3O_4(001)$. The clusters are monodisperse and seem to be randomly distributed ($V_{bias}=1.5$ V, $I_t=300$ pA). **c** STM image after CO oxidation with similar settings as in (**a**). Besides a few larger particles the clusters still seem rather monodisperse and the $Fe_3O_4(001)$ surface exhibits island formation ($V_{bias}=1.5$ V, $I_t=300$ pA)

the decreased activity for CO oxidation in the second TPR run.

Already this seemingly simple catalytic system is thus influenced by a variety of effects—from transient activity changes to restructuring—effects that could not have been identified without quantitative and reproducible TOF measurements. A careful choice of reaction parameters and a thorough characterization of the investigated catalytic system are therefore required before comparing catalysts of different composition and complexity. To achieve a reliable comparison, it is thus recommended to include cooling ramps and periods with constant temperature into the measurements and to perform measurements across the whole available range of temperatures instead of measuring TOFs only at certain temperatures.

3.3 Pulsed-Reactivity Measurements

Having established that the CO oxidation is generally controlled by reactant adsorption–desorption equilibria within the investigated pressure range, we want to further explore the individual reaction regimes, elucidate which reactant is the limiting one in different temperature regions, and gain additional insights into transient and dynamic surface processes (e.g. reactant diffusion) during the reaction. To this purpose, we utilize the pulsed-reactivity measurement mode of the sniffer setup. The two reactants are pulsed alternately onto the Pt(111) surface during two consecutive TPR heating and cooling cycles (linear ramps between 200 and 700 K with a heating rate of 1 K/s), while monitoring the CO_2 production trace. Depending on which is the limiting reactant in the respective reaction regime, the CO_2 response pulses appear either simultaneously with the CO or with the O_2 reactant pulses. The results are shown in Fig. 4, where the product pulses are color-coded according to the respective reactant they occur synchronized with: pulses synchronized with O_2 are marked in red, and pulses synchronized with CO in blue. For easier comparison, the vertical dashed lines mark the temperatures chosen in Fig. 2b and c. Note that a reactant dose of approximately 0.01 L per $C^{18}O$ pulse and 0.09 L per O_2 pulse were applied, which allows us to observe effects at the limit of a nearly empty surface. Starting from a CO pre-saturated and thus poisoned surface, we do not observe any CO_2 formation until 330 K, when CO starts to desorb. In this first regime, CO_2 production occurs exclusively during the O_2 pulses, giving clear evidence that the O_2 supply limits the reaction. The more CO desorbs, the more sites are available for the dissociative adsorption of O_2, resulting in an increased CO_2 formation with a maximum at 430 K. Finally, the CO_2 formation drops to zero at 540 K when all CO has desorbed and, due to the low reactant dosage, the O coverage is still too low to maintain a significant CO_2 production during CO pulses, as the probability that adsorbed reactants meet on the surface is negligible. From this point on, we start accumulating O atoms on the surface, and as soon as their coverage is sufficiently high, from 550 K on, we observe a sharp increase in CO_2 formation. In this regime, the reaction is CO-limited and the CO_2 production thus synchronized with the CO reactant pulses, since CO has a short residence time on the surface above its desorption temperature. Adsorbed CO either reacts with adsorbed O atoms immediately upon adsorption or desorbs again. The product formation reaches a maximum at 610 K. At higher temperatures, O starts to desorb [46], which in combination with steadily decreasing CO coverages results in a decrease in CO_2 formation. In the isothermal region, where the temperature is held constant at 700 K between the heating and cooling ramps, the CO_2 production increases continuously, which we attribute to the formation of subsurface oxygen
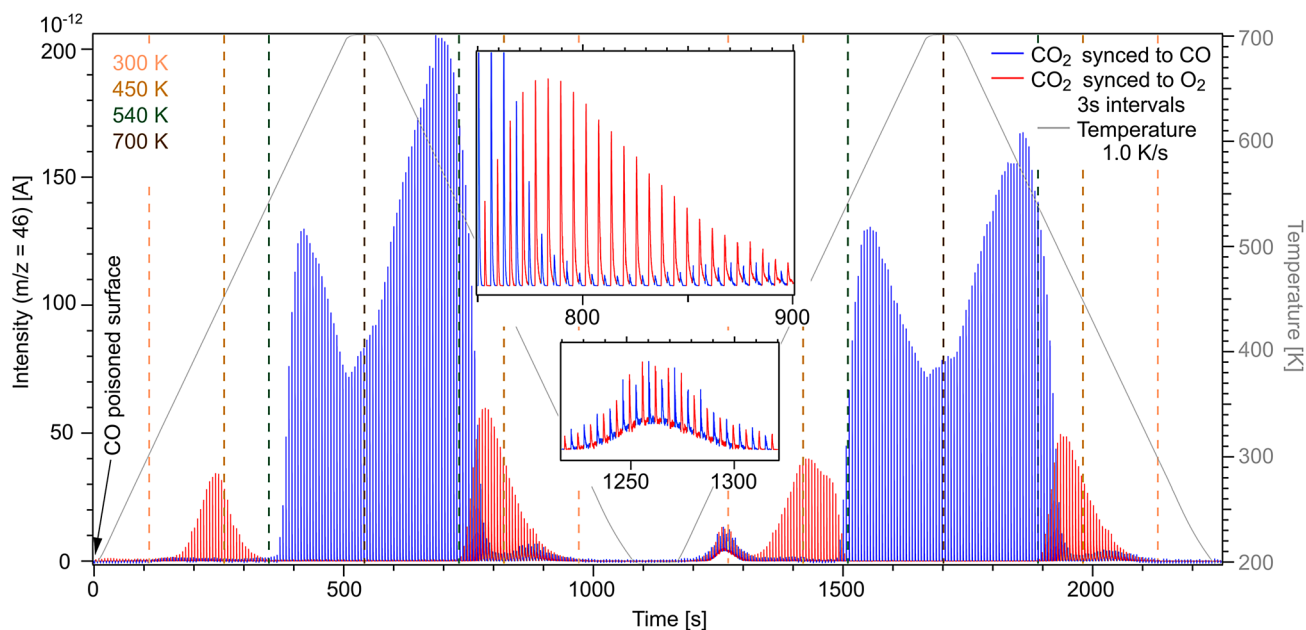
Fig. 4 $C^{16}O^{18}O$ trace (m/z = 46) during CO oxidation on Pt(111) in pulsed-reactivity measurements. O_2 and $C^{18}O$ pulses alternate in 3 s intervals during two sequential 1 K/s heating and subsequent cooling ramps. Before the measurement, the surface was saturated with $C^{18}O$ (approx. 15 L). The reactant pressures at the pulse maxima correspond to those of the continuous flow experiments in Fig. 1a. The red pulses represent $C^{16}O^{18}O$ production synchronized with O_2 reactant pulses, while the blue pulses represent $C^{16}O^{18}O$ production synchronized with $C^{18}O$ reactant pulses. The top inset shows the evolution of the O_2-synchronized product pulses at the lower end of the first cooling ramp, while the bottom inset depicts a low-temperature $C^{16}O^{18}O$ formation, which appears as a rising background underlying the product pulses synchronized with the reactant pulses at the beginning of the second heating ramp

[46] that acts as an O reservoir. Upon cooling, the CO_2 formation drastically increases again, reaching a maximum at 590 K, which shows a much higher intensity than the one during the heating ramp. We tentatively explain this high intensity to be a result of (i) subsurface oxygen diffusing to the surface, generating a continuous oxygen supply, (ii) a higher surface coverage of oxygen accumulated during the isothermal region, and (iii) lower CO-adsorption due to restructuring of the Pt surface. Once the system is cooled back down to 500 K, i.e. the upper end of the CO desorption temperature, the limiting reactant changes from CO to O_2 due to the much higher CO-coverage, resulting in a transition from CO- to O_2-synchronized CO_2 production. In contrast to the heating ramp, no gap between those two regions occurs, as sufficient O is available on the surface. The top inset in Fig. 4 is a close-up of the O_2-synchronized region. Here, a clear increase in the decay times of the product pulses with decreasing temperature can be seen. In general, the decay time of a pulse is a convolution of the pumping rate in the sniffer and transport processes on the surface. While the former is constant throughout the measurement, the latter may change depending on the current reaction regime. The change in decay times is thus indicative for slower surface diffusion of the less diffusive species, i.e. O atoms. Due to these long diffusion times, O is still present on the surface when the next CO pulse arrives, resulting in a small

additional CO-synchronized CO_2 signal. Finally, upon cooling back down to 300 K, CO_2 formation ceases completely.

In the second heating and cooling cycle, we observe exactly the same overall behavior, with the exception of two clear differences due to coverage effects: (i) Low-temperature CO_2 formation occurs at 300 K, similar to the feature observed under O_2-rich continuous measurements (Fig. 2a). A close-up of this area is shown in the bottom inset in Fig. 4. Only in this specific regime, an increased background contributes to the overall CO_2 formation in addition to the product pulses. This background signal originates from residual co-adsorbed CO and O from the previous heating and cooling cycle. As already discussed in the previous section, at these low temperatures O forms islands on the surface, with CO reacting at their perimeter [47]. This reaction takes place continuously and is thus not primarily synchronized with one specific reactant; it is not limited by mass transport from the gas phase. Instead, the reactant pulses refill the reservoir on the surface. This island formation is evident when looking at the decay times of the product pulses, superimposed onto the continuous background. For a continuous surface reaction without island formation, we would expect the increased background to result from overlapping product pulses with long decay times. In contrast, very short decay times are observed, yet the signal remains non-zero, suggesting that a fraction of the pulse refills the island reservoir, and another

fraction adsorbs and reacts directly outside the islands. (ii) The second difference between the two heating and cooling cycles appears around 540 K, where the CO_2 formation no longer drops to zero since more oxygen is available after the first run. Indeed, repeating this experiment with higher pulse pressures and thus higher reactant availability, the drop to zero is missing even in the first cycle (SI, Fig. S7), confirming our assumption that the O coverage is key, in line with comparable measurements on Pt nanoparticles [27] and clusters [21, 52].

In summary, our pulsed-reactivity measurements reveal details about the reaction mechanisms and limitations beyond those accessible through TPR experiments. We have confirmed that the low-temperature reaction peak indeed results from a reaction at the perimeter of oxygen islands. The limiting component for the overall CO_2 formation is highly dependent on the temperature. In the low temperature limit, CO poisoning results in a lack of sites for O_2 dissociative adsorption, and thus the reaction is limited by the availability of O. This changes drastically beyond the CO desorption temperature, where the reaction is first solely limited by the availability of CO molecules due to their low residence time, while at higher temperatures also the O coverage decreases, leading to an increasingly empty surface. Here, we have to distinguish between two different types of limitations: (i) External mass transport limitation of O_2 and (ii) residence time limitation of CO.

4 Discussion and Conclusionsin

In the present work, we explored the quantification of catalytic activity by TOF and conversion in order to compare UHV-based model systems of different structural complexity—specifically an extended Pt(111) surface with disperse Pt_{19} clusters on a magnetite support. While the number of active sites is well-determined in these systems, three other constraints have to be considered for the comparison of their catalytic activity, namely the influence of adsorption–desorption equilibria, mass transport limitations and particular system-dependent pressure and temperature dependencies of the reaction light-off. We tackle this experimental challenge with our pulsed sniffer setup that combines TPD with continuous (isothermal and TPR) and pulsed reactivity measurements.

Starting with the continuous reactivity measurements, we observed a perfect agreement between isothermal and TPR experiments for the CO oxidation on the extended Pt(111) surface.

On the one hand, limits of comparability with the supported cluster sample arise from the difference in structural complexity: On the extended catalytic surface, adsorbate superstructures form and make preliminary heating/cooling

cycles necessary to establish unequivocal, reproducible initial conditions for reactivity characterization. Supported clusters, in contrast, are too small for the formation of such superstructures, but instead the challenge lies in their tendency to sinter and become encapsulated. Here, the first run initially represents the activity of the bare metal particles, while SMSI-induced encapsulation sets in at high temperatures, leading to a strongly decreased catalytic activity in subsequent heating/cooling cycles.

On the other hand, particular pressure settings can trigger transient reactivity effects, which can be identified by comparing continuous TPR and isothermal measurements in a very efficient screening and we indeed found a strong influence of the CO to O_2 pressure ratio on catalytic activity. Remarkably, once a constant pressure ratio has been chosen outside of transient reactivity regimes, the variation of the total pressure leads to a highly linear TOF variation, due to an increase of the reactant coverage and this is perfectly in line with a conversion that remains constant over the full pressure range explored here.

When respecting these limits of comparability, we find a 1.6 times higher maximum TOF for the supported cluster samples than for the extended Pt(111) surface. Of course, the conversion, typically compared for the entire catalyst surface, is lower for the supported Pt clusters than for the extended Pt surface as the cluster coverage is low.

While TOF and conversion comparisons have to avoid transient reactivity regimes, pulsed measurements can help explore and map exactly these regimes and the connected mechanisms. We have identified reaction-limited reactivity regimes by pulse-independent catalytic conversion, transport limitations by different pulse decay characteristics, and associated the product formation to the limiting reactant.

Declarations

Conflict of interest The authors declare no competing financial or non-financial interest.

References

1. Kunz S, Schweinberger FF, Habibpour V, Röttgen M, Harding C, Arenz M, Heiz U (2010) Temperature dependent CO oxidation mechanisms on size-selected clusters. J Phys Chem C 114:1651–1654. https://doi.org/10.1021/jp911269z

2. Bonanni S, Aït-Mansour K, Harbich W, Brune H (2014) Reaction-induced cluster and initial size-dependent reaction rates for CO oxidation on $Pt_n/TiO_2(110)$-(1×1). J Am Chem Soc 136:8702–8707. https://doi.org/10.1021/ja502867r

3. Petzoldt P, Eder M, Mackewicz S, Blum M, Kratky T, Günther S, Tschurl M, Heiz U, Lechner BAJ (2022) Tuning strong metal-support interaction kinetics on Pt-loaded $TiO_2(110)$ by choosing the pressure: a combined ultrahigh vacuum/near-ambient pressure XPS study. J Phys Chem C 126:16127–16139. https://doi.org/10.1021/acs.jpcc.2c03851

4. Krick Calderón S, Grabau M, Óvári L, Kress B, Steinrück HP, Papp C (2016) CO oxidation on Pt(111) at near ambient pressures. J Chem Phys 144:044706. https://doi.org/10.1063/1.4940318

5. Su X, Cremer PS, Shen YR, Somorjai GA (1997) High-pressure CO oxidation on Pt(111) monitored with infrared-visible sum frequency generation (SFG). J Am Chem Soc 119:3994–4000. https://doi.org/10.1021/ja9638723

6. Dautzenberg FM (1989) Ten guidelines for catalyst testing. In: Bradley SA, Gattuso MJ, Bertolacini RJ (eds) Characterization and catalyst development. American Chemical Society, Washington

7. Chorkendorff I, Niemantsverdriet JW (2017) Concepts of modern catalysis and kinetics, 3rd edn. Wiley-VCH, Weinheim

8. Prins R, Wang A, Li X, Sapountzi F (2022) Introduction to heterogeneous catalysis, 2nd edn. World Scientific Publishing Europe Ltd., London

9. Maurer F, Beck A, Jelic J, Wang W, Mangold S, Stehle M, Wang D, Dolcet P, Gänzler AM, Kübel C, Studt F, Casapu M, Grunwaldt JD (2022) Surface noble metal concentration on ceria as a key descriptor for efficient catalytic CO oxidation. ACS Catal 12:2473–2486. https://doi.org/10.1021/acscatal.1c04565

10. Haneda M, Nakamura Y, Yamada T, Minami S, Kato N, Iwashina K, Endo Y, Nakahara Y, Iwachido K (2021) Comprehensive study of the light-off performance and surface properties of engine-aged Pd-based three-way catalysts. Catal Sci Technol 11:912–922. https://doi.org/10.1039/d0cy01952f

11. TrackAct - CRC 1441. https://www.trackact.kit.edu/. Accessed 26 Sep 2023

12. Schlögl R (2015) Heterogeneous catalysis. Angew Chem Int Ed 54:3465–3520. https://doi.org/10.1002/anie.201410738

13. Stoltze P, Nørskov JK (1985) Bridging the "pressure gap" between ultrahigh-vacuum surface physics and high-pressure catalysis. Phys Rev Lett 55:2502–2505. https://doi.org/10.1103/PhysRevLett.55.2502

14. Ertl G (2008) Reactions at surfaces: from atoms to complexity (nobel lecture). Angew Chem Int Ed 47:3524–3535. https://doi.org/10.1002/anie.200800480

15. Grunwaldt JD, Caravati M, Hannemann S, Baiker A (2004) X-ray absorption spectroscopy under reaction conditions: suitability of different reaction cells for combined catalyst characterization and time-resolved studies. Phys Chem Chem Phys 6:3037–3047. https://doi.org/10.1039/b403071k

16. Santos H, Costa M (2008) The relative importance of external and internal transport phenomena in three way catalysts. Int J Heat Mass Transf 51:1409–1422. https://doi.org/10.1016/j.ijheatmasstransfer.2007.11.005

17. Klaewkla R, Arend M, Hoelderich WF (2011) A review of mass transfer controlling the reaction rate in heterogeneous catalytic systems. In: Nakajima H (ed) Mass transfer—advanced aspects. InTech

18. Imbihl R, Ertl G (1995) Oscillatory kinetics in heterogeneous catalysis. Chem Rev 95:697–733. https://doi.org/10.1021/cr00035a012

19. Völkening S, Wintterlin J (2001) CO oxidation on Pt(111)—scanning tunneling microscopy experiments and Monte Carlo simulations. J Chem Phys 114:6382–6395. https://doi.org/10.1063/1.1343836

20. Abon M, Billy J, Bertolini JC, Tardy B (1986) Carbon on Pt(111): characterization and influence on the chemisorptive properties. Surf Sci 167:1–17. https://doi.org/10.1016/0039-6028(86)90782-X

21. Kaiser S, Maleki F, Zhang K, Harbich W, Heiz U, Tosoni S, Lechner BAJ, Pacchioni G, Esch F (2021) Cluster catalysis with lattice oxygen: tracing oxygen transport from a magnetite (001) support onto small Pt clusters. ACS Catalysis. https://doi.org/10.1021/acscatal.1c01451

22. Kaiser S, Plansky J, Krinninger M, Shavorskiy A, Zhu S, Heiz U, Esch F, Lechner BAJ (2023) Does cluster encapsulation inhibit sintering? Stabilization of size-selected Pt clusters on $Fe_3O_4(001)$ by SMSI. ACS Catal 13:6203–6213. https://doi.org/10.1021/acscatal.3c00448

23. Gänzler AM, Casapu M, Vernoux P, Loridant S, Cadete Santos Aires FJ, Epicier T, Betz B, Hoyer R, Grunwaldt JD (2017) Tuning the structure of platinum particles on ceria in situ for enhancing the catalytic performance of exhaust gas catalysts. Angew Chem Int Ed 56:13078–13082. https://doi.org/10.1002/anie.201707842

24. Zhdanov VP (1991) Arrhenius parameters for rate processes on solid surfaces. Surf Sci Rep 12:185–242. https://doi.org/10.1016/0167-5729(91)90011-L

25. McClure SM, Goodman DW (2009) New insights into catalytic CO oxidation on Pt-group metals at elevated pressures. Chem Phys Lett 469:1–13. https://doi.org/10.1016/j.cplett.2008.12.066

26. Salomons S, Hayes RE, Votsmeier M, Drochner A, Vogel H, Malmberg S, Gieshoff J (2007) On the use of mechanistic CO oxidation models with a platinum monolith catalyst. Appl Catal B Environ 70:305–313. https://doi.org/10.1016/j.apcatb.2006.01.022

27. Bonanni S, Aït-Mansour K, Hugentobler M, Brune H, Harbich W (2011) An experimental setup combining a highly sensitive detector for reaction products with a mass-selected cluster source and a low-temperature STM for advanced nanocatalysis measurements. Eur Phys J D 63:241–249. https://doi.org/10.1140/epjd/e2011-10532-7

28. Pérez-Ramírez J, Kondratenko EV (2007) Evolution, achievements, and perspectives of the TAP technique. Catal Today 121:160–169. https://doi.org/10.1016/j.cattod.2007.01.001

29. Summers RL (1969) Empirical observations on the sensitivity of hot cathode ionization type vacuum gages. National Aeronautics and Space Administration, Washington D.C.

30. AML (2022) AIGxG Ion gauge user manual. Arun Microelectronics Ltd, Pulborough

31. InstruTech (2011) Hot cathode ionization vacuum gauge manual. InstruTech Inc, Longmont

32. Ertl G, Neumann M, Streit KM (1977) Chemisorption of CO on the Pt(111) surface. Surf Sci 64:393–410. https://doi.org/10.1016/0039-6028(77)90052-8

33. Han G, Song HC, Kim SH, Park JY (2023) Role of the support oxidation state on the catalytic activity of two-dimensional Pt/TiO_x catalysts. J Phys Chem C 127:4096–4103. https://doi.org/10.1021/acs.jpcc.2c08935

34. Heiz U, Vanolli F, Trento L, Schneider WD (1997) Chemical reactivity of size-selected supported clusters: an experimental setup. Rev Sci Instrum 68:1986–1994. https://doi.org/10.1063/1.1148113

35. Klapetek P, Nečas D (2019) Gwyddion. http://gwyddion.net/. Accessed 29 Sep 2023

36. Heiz U, Sanchez A, Abbet S, Schneider WD (1999) Catalytic oxidation of carbon monoxide on monodispersed platinum clusters: each atom counts. J Am Chem Soc 121:3214–3217. https://doi.org/10.1021/ja983616l

37. Boubnov A, Dahl S, Johnson E, Puig Molina A, Bredmose Simonsen S, Morales Cano F, Helveg S, Lemus-Yegres LJ, Grunwaldt JD (2012) Structure-activity relationships of Pt/Al_2O_3 catalysts for CO and NO oxidation at diesel exhaust conditions. Appl Catal B Environ 126:315–325. https://doi.org/10.1016/j.apcatb.2012.07.029

38. Wettergren K, Schweinberger FF, Deiana D, Ridge CJ, Crampton AS, Rötzer MD, Hansen TW, Zhdanov VP, Heiz U, Langhammer C (2014) High sintering resistance of size-selected platinum cluster catalysts by suppressed ostwald ripening. Nano Lett 14:5803–5809. https://doi.org/10.1021/nl502686u

39. Hansen TW, Delariva AT, Challa SR, Datye AK (2013) Sintering of catalytic nanoparticles: particle migration or ostwald ripening? Acc Chem Res 46:1720–1730. https://doi.org/10.1021/ar3002427

40. Wan Q, Hu S, Dai J, Chen C, Wei-Xue L (2019) First-principles kinetic study for ostwald ripening of late transition metals on TiO_2(110). J Phys Chem C 123:1160–1169. https://doi.org/10.1021/acs.jpcc.8b08530

41. Gao F, Wang Y, Cai Y, Goodman DW (2009) CO oxidation on Pt-group metals from ultrahigh vacuum to near atmospheric pressures. 2. palladium and platinum. J Phys Chem C 113:174–181. https://doi.org/10.1021/jp8077985

42. Blomberg S, Hejral U, Shipilin M, Albertin S, Karlsson H, Hulteberg C, Lömker P, Goodwin C, Degermann D, Gustafson J, Schlueter C, Nilsson A, Lundgren E, Amann P (2021) Bridging the pressure gap in CO oxidation. ACS Catal 11:9128–9135. https://doi.org/10.1021/acscatal.1c00806

43. Campbell CT, Ertl G, Kuipers H, Segner J (1980) A molecular beam study of the catalytic oxidation of CO on a Pt(111) surface. J Chem Phys 73:5862–5873. https://doi.org/10.1063/1.440029

44. Wintterlin J, Schuster R, Ertl G (1996) Existence of a "hot" atom mechanism for the dissociation of O_2 on Pt(111). Phys Rev Lett 77:123–126. https://doi.org/10.1103/PhysRevLett.77.123

45. Campbell CT, Ertl G, Kuipers H, Segner J (1981) A molecular beam investigation of the interactions of CO with a Pt(111) surface. Surf Sci 107:207–219. https://doi.org/10.1016/0039-6028(81)90621-X

46. Bashlakov DL, Juurlink LBF, Koper MTM, Yanson AI (2012) Subsurface oxygen on Pt(111) and its reactivity for CO oxidation. Catal Lett 142:1–6. https://doi.org/10.1007/s10562-011-0730-z

47. Wintterlin J, Völkening S, Janssens TVW, Zambelli T, Ertl G (1997) Atomic and macroscopic reaction rates of a surface-catalyzed reaction. Science 278:1931–1934. https://doi.org/10.1126/science.278.5345.1931

48. Kinne M, Fuhrmann T, Zhu JF, Whelan CM, Denecke R, Steinrück HP (2004) Kinetics of the CO oxidation reaction on Pt(111) studied by in situ high-resolution x-ray photoelectron spectroscopy. J Chem Phys 120:7113–7122. https://doi.org/10.1063/1.1669378

49. Gänzler AM, Casapu M, Maurer F, Störmer H, Gerthsen D, Ferré G, Vernoux P, Bornmann B, Frahm R, Murzin V, Nachtegaal M, Votsmeier M, Grunwaldt JD (2018) Tuning the Pt/CeO_2 interface by in situ variation of the Pt particle size. ACS Catal 8:4800–4811. https://doi.org/10.1021/acscatal.8b00330

50. Gänzler AM, Casapu M, Doronkin DE, Maurer F, Lott P, Glatzel P, Votsmeier M, Deutschmann O, Grunwaldt JD (2019) Unravelling the different reaction pathways for low temperature CO oxidation on Pt/CeO_2 and Pt/Al_2O_3 by spatially resolved structure-activity correlations. J Phys Chem Lett 10:7698–7705. https://doi.org/10.1021/acs.jpclett.9b02768

51. Bliem R, Van Der Hoeven J, Zavodny A, Gamba O, Pavelec J, De Jongh PE, Schmid M, Diebold U, Parkinson GS (2015) An atomic-scale view of CO and H_2 oxidation on a Pt/Fe_3O_4 model catalyst. Angew Chem 127:14205–14208. https://doi.org/10.1002/anie.201507368

52. Bonanni S, Aït-Mansour K, Harbich W, Brune H (2012) Effect of the TiO_2 reduction state on the catalytic CO oxidation on deposited size-selected Pt clusters. J Am Chem Soc 134:3445–3450. https://doi.org/10.1021/ja2098854